Received: 25 March 2022 | Accepted: 13 October 2022

DOI: 10.1111/2041-210X.14023

Methods in Ecology and Evolution

RESEARCH ARTICLE

Using cloud radar to investigate the effect of rainfall on migratory insect flight

Charlotte E. Wainwright[1] | Sabrina N. Volponi[1] | Phillip M. Stepanian[1] | Don R. Reynolds[2,3] | David H. Richter[1]

[1]Department of Civil & Environmental Engineering & Earth Sciences, University of Notre Dame, Notre Dame, Indiana, USA

[2]Natural Resources Institute, University of Greenwich, Kent, UK

[3]Rothamsted Research, Harpenden, UK

Correspondence
Charlotte E. Wainwright
Email: cwainwri@nd.edu

Present address
Phillip M. Stepanian, MIT Lincoln Laboratory, Lexington, Massachusetts, USA

Funding information
National Science Foundation Graduate Research Fellowship, Grant/Award Number: NSF DGE-1841556; Richard and Peggy Notebaert Premier Fellowship; National Science Foundation Division of Emerging Frontiers, Grant/Award Number: 1840230

Handling Editor: Sydne Record

Abstract

1. The fate of migrating insects that encounter rainfall in flight is a critical consideration when modelling insect movement, but few field observations of this common phenomenon have ever been collected due to the logistical challenges of witnessing these encounters. Operational cloud radars have been deployed around the world by meteorological agencies to study precipitation physics, and as a byproduct, provide a rich database of insect observations that is freely available to researchers. Although considered unwanted 'clutter' by the meteorologists who collect the data, the analysis method presented here enables ecologists to delineate co-occurring signals from insects and raindrops.
2. We present a method that uses image processing techniques on cloud radar velocity spectra to examine the fate of migrating insects when they encounter precipitation. By analysing velocity spectra, we can distinguish flying insects from falling rain and compare the relative density of insects in flight before, during and after the rainfall. We demonstrate the method on a case of insect migration in Oklahoma, USA.
3. Using this method, we show the first reconstructed images of migrating insect layers in flight during rainfall. Our analysis shows that mild to moderate rainfall diminishes the number of insects aloft but does not cause full termination of migratory flight, as has previously been suggested.
4. We hope this technique will spur further investigations of how changing weather conditions impact insect migration, and enable some of the first of such studies in regions of the world that are underrepresented in the literature.

KEYWORDS
entomology, flight behaviour, image processing, radar aeroecology

1 | INTRODUCTION

Seasonal long-distance migration of insects involves the mass movement of trillions of individuals, representing huge fluxes of nutrients and energy (Hu, Lim, Horvitz, et al., 2016). These movements can span continental scales, linking disparate populations, communities and ecosystems through the systematic exchange of interacting materials and organisms that might not otherwise exist in proximate environment patches (Leibold et al., 2004). Despite the importance of insect migration across a range of communities and ecosystems, it still remains relatively understudied in comparison to the migration of other taxa (Satterfield et al., 2020). This relative lack of knowledge comes in part from the logistical and technological difficulties associated with tracking such small, flying animals at high altitudes along their migration pathways.

Understanding and predicting insect migration is important for several reasons. Many species of migrating insects are crop pests of economic importance or can act as vectors of pathogens, but migrating insects can also be pollinators and predators of pests (Satterfield et al., 2020; Wotton et al., 2019). To improve predictive models of insect migration, we need both initial conditions (insect source locations) and an understanding of how insects respond to changing meteorological conditions encountered during migration (Sturtevant et al., 2013). Weather conditions impact insect migration in several ways, both in terms of take-off and landing decisions (e.g. timing, fly/no-fly decisions), as well as responses in flight after encountering a change in conditions. For example, temperature is known to have a strong influence on insect flight, as insects require an ambient threshold temperature for take-off. The effect of temperature once the insects are aloft is more difficult to investigate, but generally few insects are recorded flying at temperatures below 10°C (Drake & Reynolds, 2012), although there are occasional records of large insects in flight at temperatures as low as 5°C (Drake & Farrow, 1985).

Wind is also a key factor in insect migration (Reynolds et al., 2018). Many insects migrate at altitudes of several 100 m or more and exploit favourable winds to reduce the energy expenditure required for long-distance movements (Hu, Lim, Reynolds, et al., 2016). Besides transporting insects over long distances, certain wind patterns such as sea breeze fronts, low-level jets and convective storm outflow boundaries can cause localized high concentrations of insects (Burt & Pedgley, 1997; Drake, 1982, 1985; Russell & Wilson, 1997).

Beyond temperature and wind patterns, rainfall is one of the most disruptive forces in long-distance insect migration (Reynolds et al., 2018). Encountering rainfall while in flight could potentially be the dominant cause in cases where migrating insects cease flying en masse, and this effect can lead to highly localized aggregations of insects at ground level (Greenbank et al., 1980); this, in turn, can lead to serious outbreaks of pest species (Drake & Reynolds, 2012). Compared to the effects of temperature and wind, the impact of rain on insect flight is less well understood (but see discussions in Drake and Reynolds (2012) and Reynolds et al. (2018)).

One of the few direct observations of insect behaviour when encountering rain during migratory flight comes from Dickison et al. (1986), who reported that spruce budworm moths not only continued flying in the clear air between storm cells but were also observed flying in heavy rain within the cells at an altitude of ≈400 m. The moths were only able to be identified and observed in situ by illuminating aircraft landing lights while in flight, highlighting the practical difficulties in observing insect migration aloft in the rain.

Most of the remaining studies on how insects respond to precipitation come from laboratory experiments in which high-speed photography was used to examine raindrops falling on insects (Dickerson et al., 2012, 2014). These experiments defined three potential outcomes of individual insect–raindrop collisions depending upon the relative mass and size of the raindrop (m_1, R_1) to the insect (m_2, R_2). A raindrop can either remain intact while accelerating the insect downwards ('push' mode), which occurs for small and light insects with $m_2 / m_1 \ll 1$ and $R_2 / R_1 \leq 1$ such as gnats or mosquitoes. The droplet can also surround the insect, encasing it in water ('coat' mode), which theoretically occurs for $m_2 / m_1 \geq 1$ and $R_2 / R_1 \leq 1$, but experiments suggest would only rarely occur for free-flying insects due to the high relative density of water compared to insects of comparable size. For very small insects (e.g. parasitic wasps: 0.03 mg) encapsulation by a droplet would probably be fatal. The third 'splash' mode, in which the droplets fragment upon impact with the insect, occurs for $m_2 / m_1 > 1$ and $R_2 / R_1 \gg 1$ (large or heavy insect, small or light raindrop) and is theorized to apply to most medium or large insects such as hoverflies, moths, butterflies and beetles. Considering a 2-mm raindrop, insects with mass below 2 mg will be pushed, but larger insects will be splashed (Dickerson et al., 2014). The effect of rainfall on insects in flight will also vary depending on the rainfall rate, raindrop number concentration and insect flight speed, as these all affect the chance of an insect colliding with a raindrop.

Other information on insect behaviour during rainfall comes from radar studies. Over the past several decades, the use of radar to study insect movements has expanded and developed into the standalone field of study of radar entomology (Drake & Reynolds, 2012). Specialized entomological radars have been developed that can monitor the movement of individual insects, providing information on the insect speed, size and direction of motion. These radars have provided new insights into a range of migratory flight behaviours (Chapman et al., 2003, 2011; Drake, 1985; Hu, Lim, Reynolds, et al., 2016) but remain limited in spatial coverage and cannot provide surveillance when precipitation is present.

Aggregations of insects are also visible on weather surveillance radars (WSRs). Recent advances in WSR technology have allowed great strides in radar aeroecology for studying insect movement and behaviour (e.g. Boulanger et al., 2017; Stepanian et al., 2020; Tielens et al., 2021), as well as making use of insect bioscatter to infer flow features in otherwise clear air (e.g. Banghoff et al., 2018, 2020). Upgrades to WSR technology have enabled clear delineation between biological and meteorological echoes on these radars, with precipitation having high co-polar cross-correlation coefficient (ρ_{HV}) values of ≥ 0.9 and bioscatter having a much lower value (see Stepanian et al., 2016, for details on polarimetric

WSR products like ρ_{HV} and their use in ecology). Biological taxa can also be determined, as many insect taxa produce strong symmetrical patterns in differential reflectivity (Z_{DR}) during periods of migratory flight in an aligned orientation, with very high Z_{DR} maxima due to the insects' elongated body shape in horizontal flight (Jatau et al., 2021; Melnikov et al., 2015; Rennie, 2014; Stepanian et al., 2016).

Previous studies using WSR have shown that insect migration continued in the clear air between convective rain cells (e.g. Browning et al., 2011; Leskinen et al., 2011; Markkula et al., 2008). There are also several reports of high insect catches immediately following storms and heavy rainfall (e.g. Dickison et al., 1983; Greenbank et al., 1980), but it is unclear whether the insects are grounded by direct collisions with raindrops, brought down by downdrafts or choose to descend due to changing temperature, winds or pressure levels. Depending on the synoptic setup and type of rainfall, it may be difficult to disentangle the effects of precipitation from those caused by corresponding changes in temperature or wind speed and direction.

Vertically pointing millimetre-wavelength radars (commonly known as cloud radars) have also been used to study insect motion (Geerts & Miao, 2005a; Wainwright et al., 2017, 2020; Wood et al., 2009), and while their wavelength means they can observe even single insects at altitudes of several hundreds of metres, they are less widespread than WSRs. However, cloud radars have been deployed around the world (see Figure 1) including in many places where insects are regularly present in the boundary layer for some or all of the year. There is considerable interest in the meteorological community in discriminating the cloud radar signal caused by insects, clouds and precipitation. For researchers interested in clear-air vertical velocity, the additional velocity provided by insects is a source of clutter that must be accounted for and mitigated (Chandra et al., 2010; Geerts & Miao, 2005b). Increasingly sophisticated methods to identify and remove insect clutter have

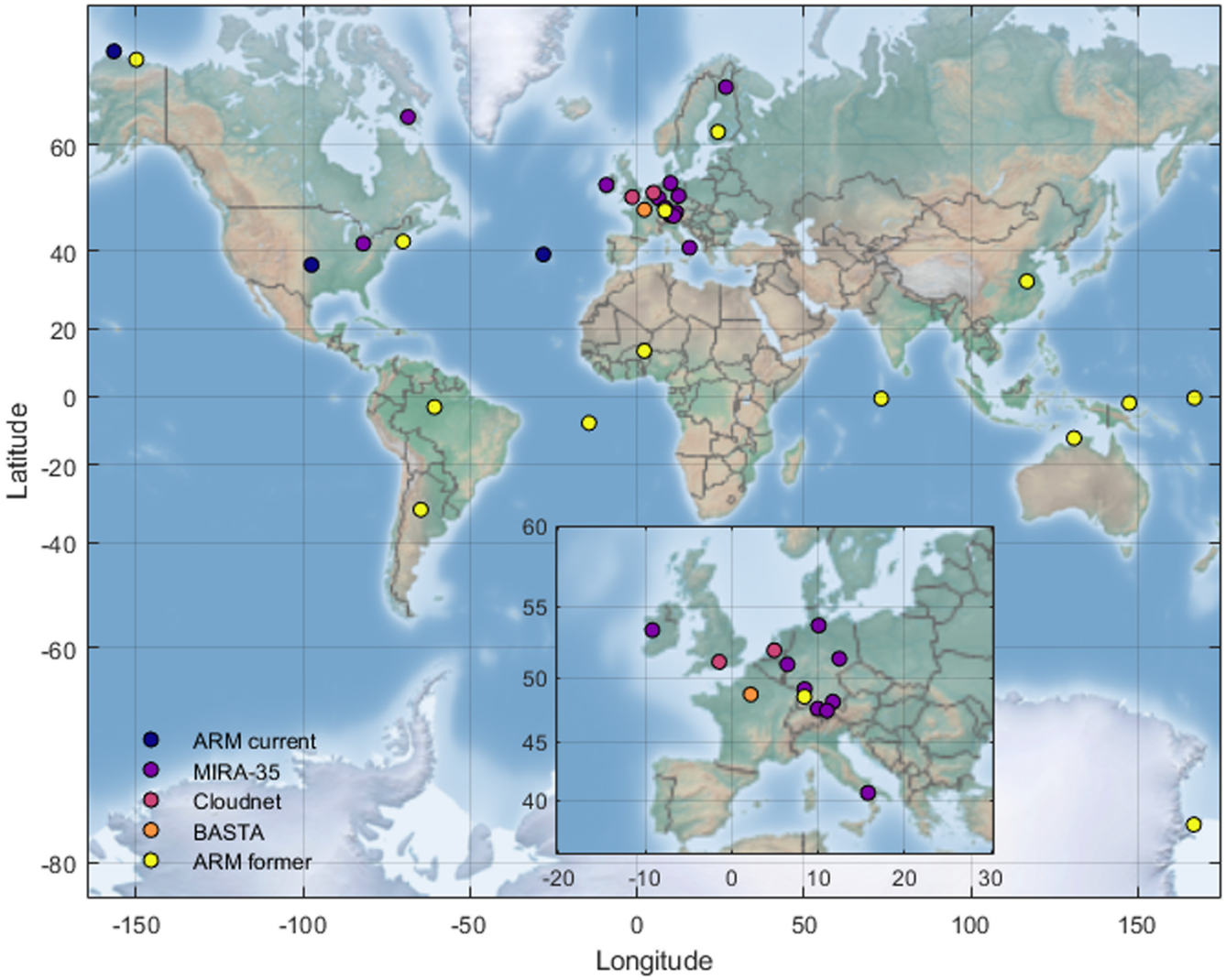

FIGURE 1 Map showing the location of millimetre-wavelength (including Ka- and W-band) cloud radars around the world. The inset map highlights the radar locations in Europe. Radars shown include those operated by the US Department of Energy's Atmospheric Radiation Measurement at current fixed sites and during prior field campaigns (Kollias et al., 2016), those in the Cloudnet program (Illingworth et al., 2007), the BASTA radar (Delanoë et al., 2016; a Ka-band radar is collocated at this site) and the commercially available MIRA-35 radars.

been developed (see e.g. Kalapureddy et al., 2018; Luke et al., 2008; Williams et al., 2018, 2021). Generally, these algorithms delineate range gates containing insects, clouds, an insect/cloud mix or precipitation. No prior efforts have examined the insect/rain mix which is the focus of this study, or investigated insect and cloud or precipitation mixes through the lens of insect behaviour.

For each radar type mentioned here, the reflectivity from insects is completely masked by precipitation in everything except the lightest rain. This is caused by the high relative number concentration of raindrops to insects within a radar volume, resulting in much higher reflectivity from the precipitation even for large insects. Here we describe a method that uses spectral analysis of cloud radar observations to distinguish insects from falling rain within a single sampling volume. By separating the portion of the signal resulting from insects from collocated precipitation, vertically pointing cloud radars can reveal how the relative density of insects aloft is affected by rainfall. Section 2 describes the spectral processing method, and Section 3 demonstrates the method on an example case. Section 4 discusses the limitations of this method as well as the potential for future extensions of this work, and conclusions are given in Section 5.

2 | METHOD

The method described here has been developed for use on Doppler velocity power spectra data from vertically pointing cloud radars. A map showing the locations of current and former deployments of cloud radars is shown in Figure 1. Radars have been deployed on every continent, and the number of sites grows each year. Data from many of the research radars are available to the public at no cost (e.g. all data from the Atmospheric Radiation Measurement program cloud radars).

Fundamentally, the method involves splitting the power spectra at each range gate into contributions from insects and precipitation, based on radial velocity, v (i.e. scatterer fall speed). The method is fairly simple, and only requires the user to select a velocity threshold value that is used to delineate insects from falling rain. The steps involved in the method are listed below, and the method is illustrated graphically in Figure 2 and demonstrated using data from a Ka-band zenith-pointing radar (KAZR) located at the Department of Energy's Atmospheric Radiation Measurement program Southern Great Plains (ARM SGP) site in northern Oklahoma, USA in Figure 3. More details about the radar are included in Section 3.

1. Dealias velocity spectra

If the vector sum of the raindrop fall speeds and any background vertical motion is greater than the Nyquist velocity of the radar, a phenomenon known as velocity aliasing occurs that yields an error in the velocity spectrum (Doviak & Zrnić, 1993). In cases where this occurs, the velocity spectrum must first be dealiased, correcting the resulting shift in velocities (as shown in step 1 in Figure 2). For the radar data shown in Figure 3 the Nyquist velocity is 5.96 m/s, and all velocities outside of ±5.96 m/s would be shifted to the opposite side of the spectrum. Examples showing dealiased radial velocity are seen in Figure 3a–c.

2. Remove background noise

The background noise level for each range gate is found by applying the Hildebrand–Sekhon algorithm (Hildebrand & Sekhon, 1974) to each individual Doppler velocity spectrum. All signals falling below the critical signal-to-noise ratio are set to zero, and the remaining signal is set to a value of 1. This process is repeated for each range gate in turn, resulting in a binary signal and noise image at each timestep (step 2 in Figures 2 and 3d).

3. Group contiguous pixels

Once the data have been reduced to a binary signal and noise image, we group the pixels into contiguous blocks of signal separated by noise. Pixels above the noise threshold that are adjacent in radial velocity or range are grouped into a single component (step 3 in Figures 2 and 3e), which is assigned a unique identifying number. This procedure is known as connected component labelling or blob colouring.

4. Calculate statistics on each pixel group

After splitting the data into connected components or blobs, statistics can be calculated on each blob. We find the centroid of each blob, as well as the maximum and minimum vertical velocity contained within it, as indicated by the vertical dashed blue and red lines in step 4 of Figure 2. Additional statistics for each blob can be calculated as needed (e.g. texture parameters or polarimetric variables such as linear depolarization ratio (LDR), see discussion in Section 4).

5. Separate blobs based on threshold velocity

Select a threshold velocity value (v_t) that will be used to delineate insects and falling rain. If the blob minimum $v \geq -v_t$ and the blob maximum $v \leq v_t$, then the blob is classified as insects. This is illustrated by the dashed black line in step 5 of Figure 2 and demonstrated in Figure 3 for a v_t value of ± 1 m/s (i.e. the blobs falling between the dashed black lines in Figure 3e are classified as insects, and the remaining blobs are classified as precipitation). These thresholds can be determined by visual inspection of the location of the velocity value associated with the gap between the precipitation and insect blobs (Figure 3e).

6. Calculate reflectivity from insect and precipitation components

Based on the blob classifications from the previous step, the reflectivity from blobs classified as insects and precipitation can be

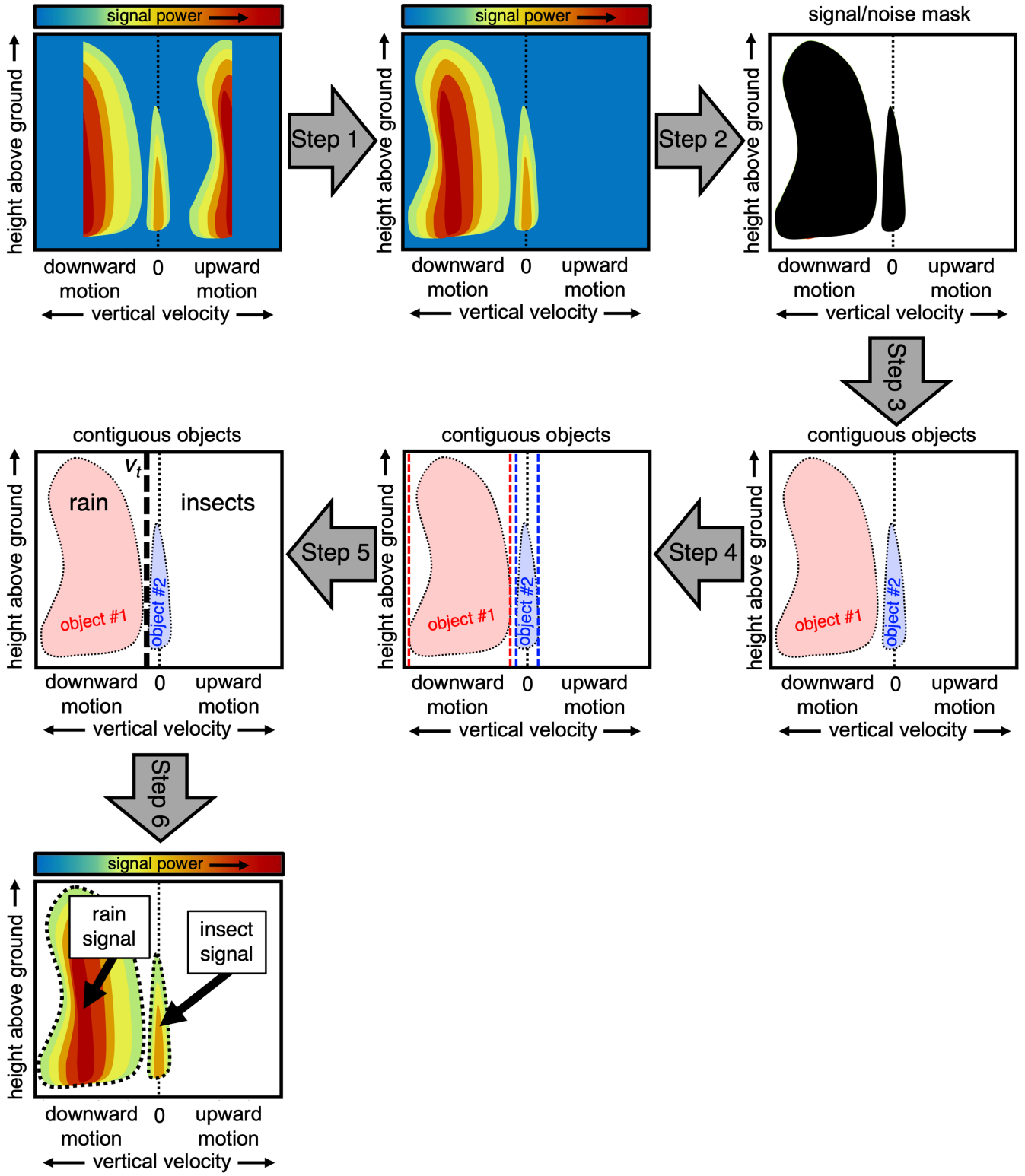

FIGURE 2 A schematic illustrating the steps of the method as outlined in Section 2.

summed separately for each range gate and a time–height profile of insect reflectivity can be constructed.

The connected component labelling method here has previously been used to identify bioscatter on WSR data, and the method used here was developed based on Stepanian et al. (2014). The method has been developed for vertically pointing millimetre-wavelength radars, and in the next section the method is applied to an example case.

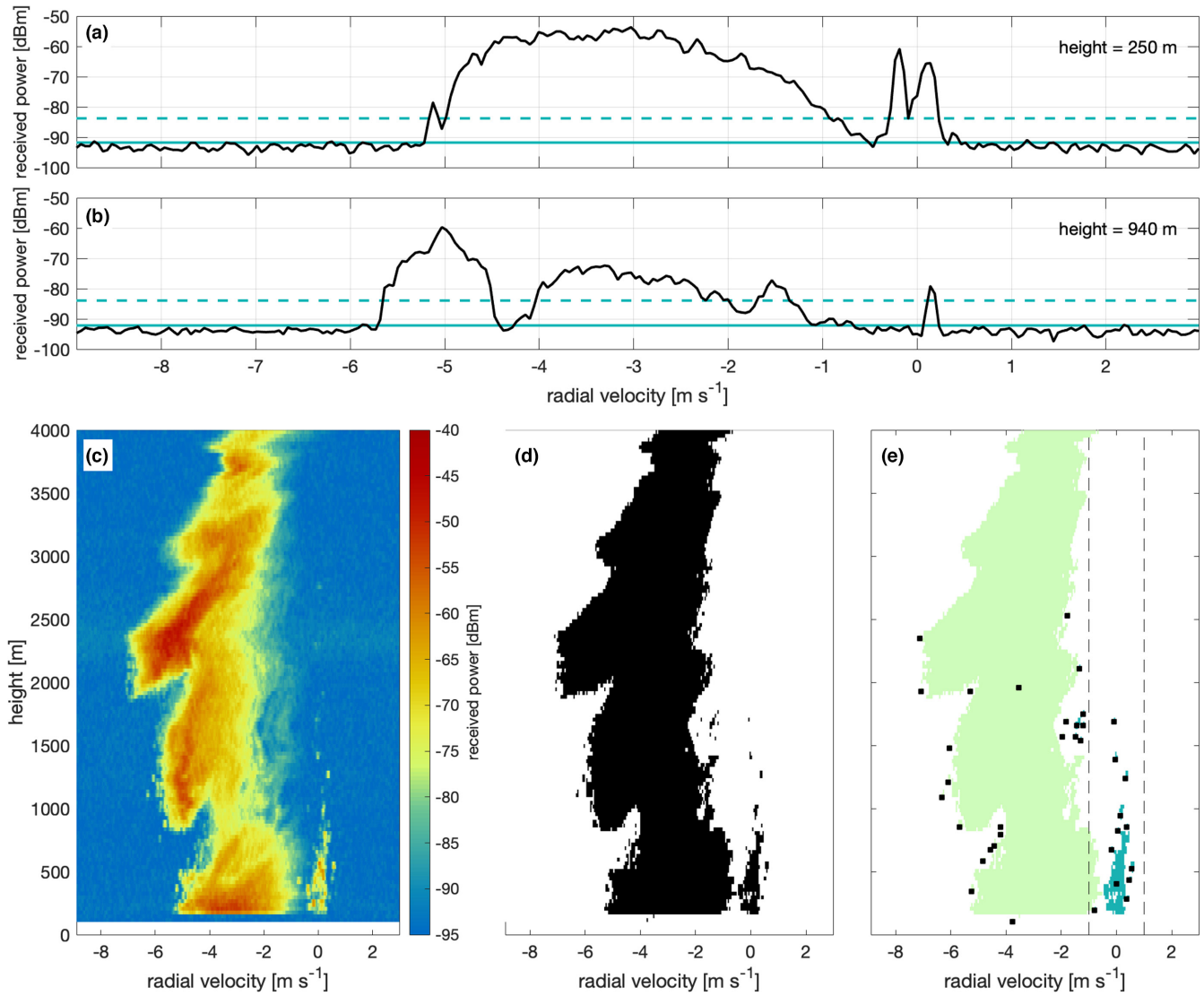

FIGURE 3 (a) and (b) show dealiased radial velocity spectra at heights of 250 and 940 m, respectively, and the solid and dashed lines show the mean noise and maximum noise floor at each height. (c) Radial velocity spectra at heights below 4 km at a single time. (d) Binary image after background noise removal. (e) Individual connected components remaining in the signal, with the centroid of each component indicated by the black square. Vertical dashed lines are velocity filters of −1 and 1 m/s.

3 | CASE STUDY

For the example case, we use data from the KAZR which forms part of a suite of meteorological instrumentation installed at the ARM SGP site (Sisterton et al., 2016) in Lamont, Oklahoma, USA (36.605°N, 97.486°W, altitude 314 m). The radar operates at 35 GHz (8.6 mm wavelength), and it has a 3-dB beamwidth of 0.19°. It generally operates in a vertical stare mode, and the raw co-polar and cross-polar Doppler velocity power spectra are transformed into time–height profiles of co-polar and cross-polar reflectivity (Z_c and Z_x), vertical velocity (v_c and v_x) and spectrum width, with a 30 m height interval in the boundary layer and 3.7 s update time. More information on polarimetric radar products and their use in ecology can be found in several primers (e.g. Stepanian et al., 2016). KAZR is designed to study cloud particles and so is highly sensitive at low reflectivities, with a minimum detectability threshold of −114 dBZ at the lowest range gates. The high sensitivity to low reflectivities means that millimetre-wavelength radars (e.g. Ka- and W-band) can see small insects that may not be detectable by radars operating at S-band or X-band (Franck et al., 2021).

During warm weather, cloud radar returns in the boundary layer are dominated by insects at the SGP site (Luke et al., 2008), which has 'profound implications for shallow cloud studies' (Lamer & Kollias, 2015). As such, significant effort has been made towards identifying and removing insect returns from the cloud radar data (e.g. Luke et al., 2008; Williams et al., 2021). While insects are clutter for cloud studies, insect returns can also be used to explore insect behaviour under different atmospheric conditions (e.g. Wainwright et al., 2017, 2020; Wood et al., 2009). Insect returns on cloud radars can also be used to estimate the clear-air convective boundary layer height (Franck et al., 2021).

Here we seek to illustrate the effect of rainfall on insects in flight by investigating a case from 30th July 2015. We use the KAZR time–height co-polar reflectivity (Z_c) profile to identify times with both insect migration and precipitation. Falling rain is clearly visible as regions of high Z_c and strongly negative (i.e. downward) radial velocity which descend from a cloud layer above. Insect migration can be identified as a layer of increased reflectivity aloft that remains at a relatively constant height for a period of time. Layers of migrating insects can be differentiated from cloud layers based on polarimetric variables such as LDR (Martner & Moran, 2001), or by incorporating additional data from WSRs as described below.

To ensure that there is a bioscatter layer present over the SGP site, and that this is mainly comprised of insects (rather than birds or other biota), we examine data from the US national WSR network (Figure 4). High Z_{DR} values of ≥7 dB can be seen in Figure 4 at 13:00 UTC, indicating that commonly aligned insects are present in the airspace prior to the precipitation. Rain approaches from the north-west side of the SGP site (radar location indicated by the black dot in Figure 4), and by 15:00 UTC an outflow boundary from the convective system is visible to the south and south-east of the SGP site. The high reflectivity in the outflow boundary is comprised of biological scatterers, as indicated by the low co-polar cross correlation coefficient (ρ_{HV}), and these are most likely insects due to the prevalence of high Z_{DR} in the area around the outflow boundary. Z_{DR} within the outflow boundary itself is reduced by several dB from the surrounding biological signal indicating that insects caught within the outflow boundary are more randomly aligned (as noted by Greenbank et al., 1980). The area of bioscatter ahead of and behind the outflow boundary continues to have high Z_{DR}, which suggests that commonly aligned insect migration is continuing throughout the area.

Figure 5 shows the KAZR time–height reflectivity plot. Initial insect migration between 1 and 2 km is clearly visible, as well as two periods of rain (16:45–17:15 and 18:15–20:00 UTC). Figure 5b–e shows the velocity power spectra at four times, two without rain (Figure 5b,d) and two during rain (Figure 5c,e). Figure 5b shows the velocity spectra at 16:05 UTC, before rain begins. Insect signal is visible below 500 m and in a layer around 1500 m, indicated by increased reflectivity with radial velocity centred around zero at those heights. By 17:05 UTC, rain has reached the site, shown by the large connected region of high reflectivity with strongly downward vertical velocity (Figure 5c). This cycle is repeated in Figure 5d and e, with insect migration continuing at 1500 m at 18:00 UTC (Figure 5d) prior to another period of rain. By 19:00 UTC, heavier rain has begun, as shown by the higher reflectivity and high maximum downward radial velocities. During all four times shown in Figure 5b–e, evidence of the elevated insect migration persists. This is examined in more detail in Figure 6.

The persistent layer of insects migrating in an isolated altitudinal band around 1500 m above-ground level is especially interesting because individual insects seem to be responding to proximate atmospheric conditions in a consistent manner, for example, maintaining a common, preferred flight altitude. Because of this behavioural consistency, we can examine this portion of the signal in more detail by averaging the velocity spectra between 1400 and 1600 m and examining how the averaged spectra changes over time (Figure 6). The periods of rain visible in Figure 5 are clearly seen in the averaged velocity spectra and averaged reflectivity, and the insect signal is seen oscillating around zero radial velocity (i.e. level flight). Insect migration continues during the two periods of rain from 16:55–17:25 to 18:12–18:42 (Figure 6c,d), with the insect signal at a radial velocity of around zero continually visible. Around 18:35, the rain becomes heavier, indicated by the increased received power at higher maximum downward vertical velocities and the increased reflectivity (Figure 6b). As the rain intensity increases, it becomes more difficult to pick out the insect signal as the noise floor increases (Figure 6d,e). The increase in the noise floor during heavier rain is also seen in Figure 6e at around 19:05 UTC. Further increases in the rainfall intensity at 19:14 UTC increase the noise floor even higher and the insect signal can no longer be distinguished. Once the noise floor returns to pre-precipitation levels at 19:18 UTC, the insect signal is no longer visible and it does not reappear until after the precipitation has ended.

We apply the method outlined in Section 2 to the case study, using three different values of v_t (±0.5, ±1 and ±2 m/s) arbitrarily chosen to highlight the impact of this velocity threshold on partitioning reflectivity to either insects or precipitation. Figure 7a shows the total reflectivity which includes contributions from insects, precipitation and noise (as in Figure 5a). The lower panels show the corresponding reflectivity when only blobs classified as insects are included, with $v_t = \pm 2$ m/s (Figure 7b), $v_t = \pm 1$ m/s (Figure 7c) and $v_t = \pm 0.5$ m/s (Figure 7d). Comparing the panels of Figure 7, we see that using a higher v_t value results in some rainfall signal being misclassified as insects, particularly during lighter rain. This is because for small droplet sizes, the droplet fall speed may be sufficiently low that it falls below v_t. However, when v_t is decreased, some of the insect signal is lost as indicated by the reduced reflectivity in Figure 7d compared to Figure 7b even when it is not raining. Regardless which v_t value is used, Figure 7 shows that some insects continue migrating around 1500 m during the period of rain from 18:15 to 19:00, although the reflectivity is reduced from before the rain. While our focus here is on insects migrating at altitude, this pattern also occurs for insects flying below 500 m (which may or may not be migrating).

It is clear from Figure 7 that the choice of v_t is very important and can strongly affect the method performance. To test the effect of v_t, we consider two separate periods of rain: that in Figure 6c, and that in Figure 6d,e combined. For both rain periods, we sum the insect reflectivity (from Figure 7c–e) over a height range of 1400–1600 m for the 30-min period before the rain starts and after it ends. We compare the reflectivity distribution from insects among the three v_t groups for four distinct time periods (pre-rain and post-rain, for two separate rain episodes). We aim to compare the reflectivity distributions between the three v_t values to understand how the choice of v_t affects the method outcome. Each reflectivity distribution was found not to be normally distributed using a goodness-of-fit test. Since we could not use a parametric ANOVA due to the reflectivity distributions being non-Gaussian, we instead used the

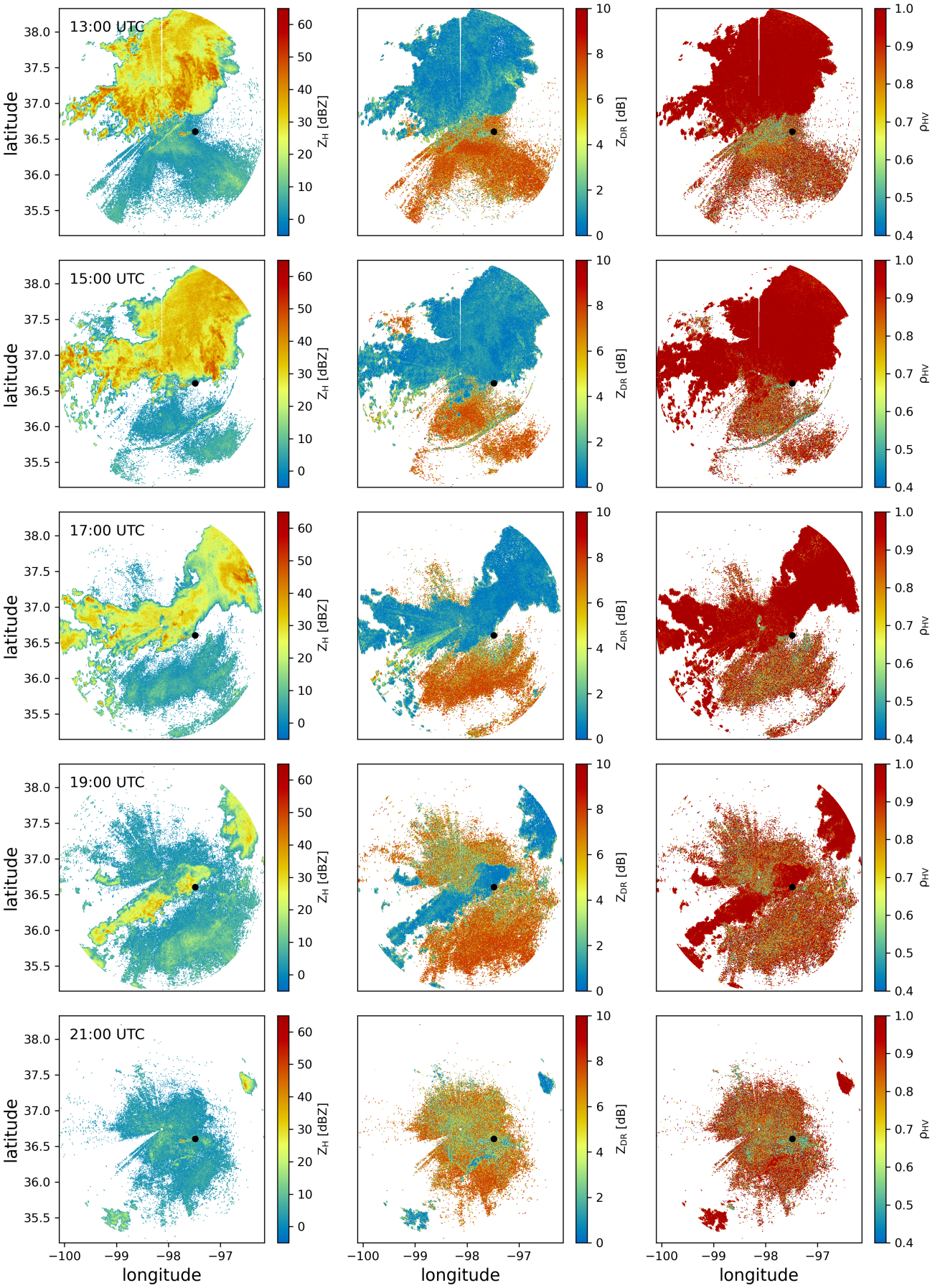

FIGURE 4 Plan position indicator (PPI) plots showing the evolution of horizontal reflectivity (Z_H, left column), differential reflectivity (Z_{DR}, middle column) and co-polar cross correlation coefficient (ρ_{HV}, right column) during the case study. Data are from the KVNX radar at Vance Air Force Base in Oklahoma. The ARM SGP site is shown by the black dot. The NEXRAD analysis and visualization were performed using Py-ART (Helmus & Collis, 2016).

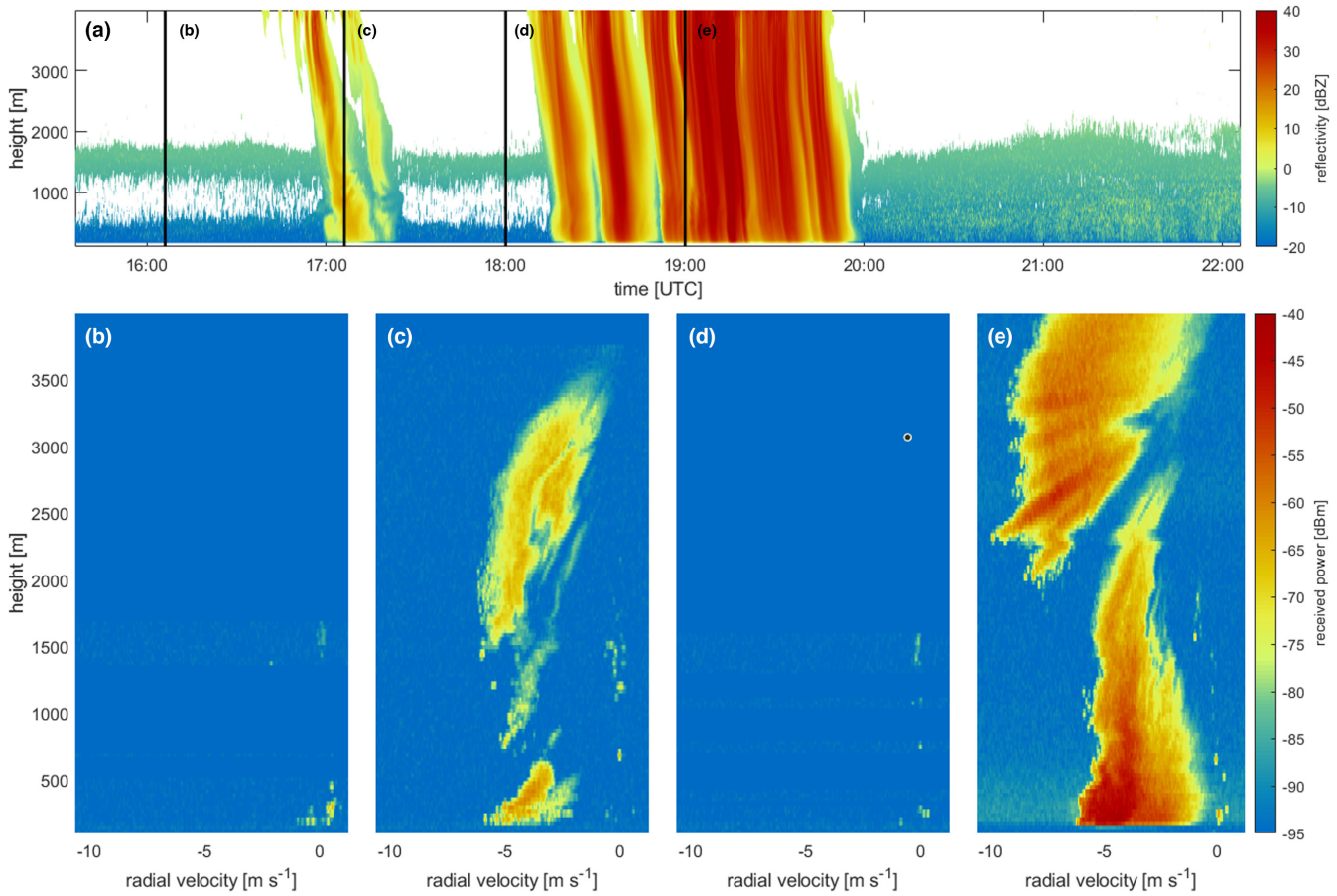

FIGURE 5 (a) A time–height profile of the co-polar reflectivity from the cloud radar at the ARM SGP site during the case study. The four lower panels show the velocity spectra at the times marked by vertical black lines in (a): 16:05 UTC (b), 17:05 UTC (c), 18:00 UTC (d) and 19:00 UTC (e); local time is UTC−5 h.

nonparametric equivalent, the Kruskal–Wallis test (MATLAB function kruskalwallis) to see whether the reflectivity distributions at a given time differ based on v_t. Post-hoc pairwise comparisons were conducted using the MATLAB function multcompare.

The choice of v_t had a significant effect on the magnitude of measured insect reflectivity in the 30 min before (Kruskal–Wallis: $H = 55.91$, $df = 2$, $p < 0.05$) and the 30 min after (Kruskal–Wallis: $H = 7.59$, $df = 2$, $p < 0.05$) the first rain event. Before the first rain event, less insect reflectivity was registered when a v_t value of 0.5 m/s was used compared to 1 m/s ($p < 0.05$) or 2 m/s ($p < 0.05$), although the mean reflectivity was not significantly different for v_t of 1 and 2 m/s ($p > 0.05$). After the rain, the measured insect reflectivity was lower with $v_t = 0.5$ m/s than with $v_t = 2$ m/s ($p < 0.05$), but neither were significantly different from when $v_t = 1$ m/s ($p > 0.05$). This analysis was repeated for the second rain event, and in this case the mean rank of the measured insect reflectivity distribution was not significantly different for the three v_t values either before or after the rain (pre-rain: Kruskal–Wallis, $p > 0.05$; post-rain: Kruskal–Wallis, $p > 0.05$). The statistical analysis was not repeated for the insect reflectivity distribution during the rain, due to the insect signal sometimes being masked by the high noise floor during rain, as seen in Figure 6d,e. If the insect signal falls below the critical signal-to-noise ratio identified by the Hildebrand and Sekhon algorithm (Hildebrand & Sekhon, 1974), then this could lead to the false impression that insect migration is completely suppressed even if it is not.

The statistical analysis reveals that the choice of v_t is indeed important, and in some cases can alter the reflectivity distribution of insects even when rain is not present by classifying insect signal as rainfall when $|v_t|$ is low. The choice of v_t is a delicate balance between excluding insects that are ascending or descending at rates greater than $|v_t|$ (whether via self-powered flight or caught in updrafts or downdrafts) and including light precipitation in the insect reflectivity. This is illustrated in Figure 7, where the v_t of 1 and 2 m/s clearly allows some precipitation to be classified as insects, while v_t

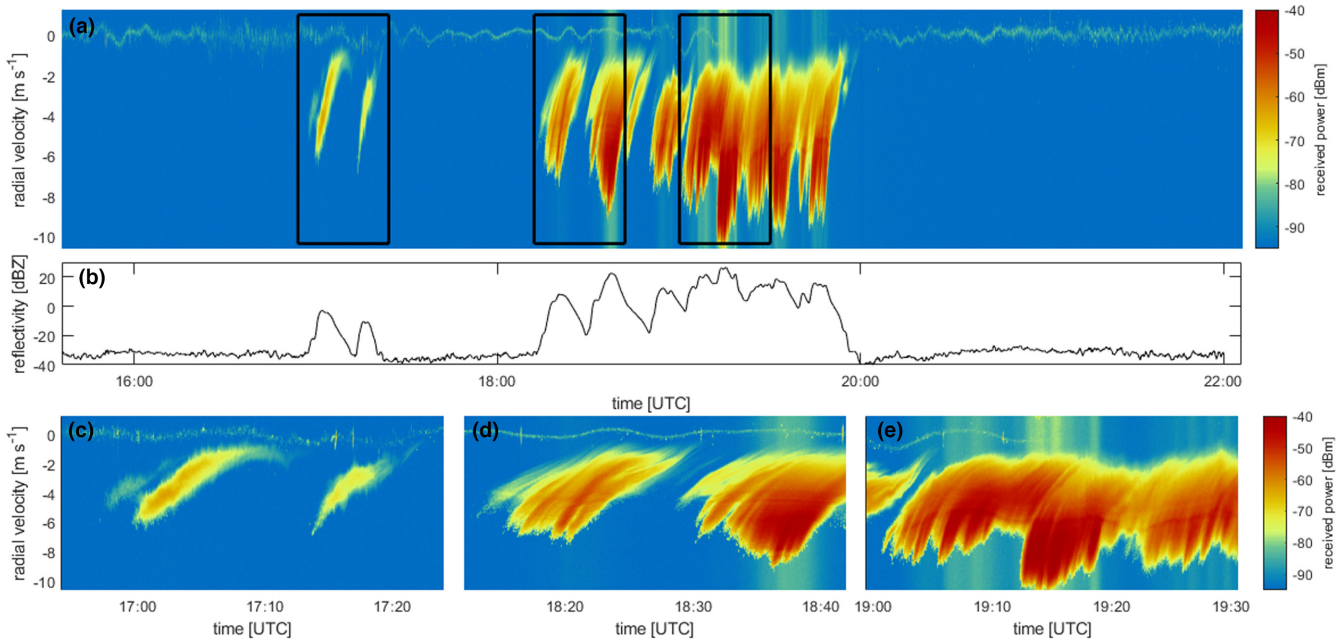

FIGURE 6 (a) Velocity spectra averaged over a height range of 1400–1600 m. (b) Reflectivity (Z_c) averaged over 1400–1600 m. The three lower panels show close-ups of the velocity spectra over three 30-min periods marked by the black boxes in (a): 16:55–17:25 UTC (c), 18:12–18:42 UTC (d), and 19:00–19:30 UTC (e). The velocity spectral power is expressed in units of dBm (power relative to 1 mW).

of 0.5 m/s removed some of the insect signal as rainfall even in clear air. As such, the 'best' choice of v_t will depend on the specifics of each case and whether the desired outcome is focused on capturing all the insect signal or excluding all the rain.

4 | DISCUSSION

Even before applying the method from Section 2, we can see from Figures 5 and 6 that insect migration does not totally stop when insects aloft encounter rain. Once the method has been applied, Figure 7 indicates that the layer structure of migrating insects aloft remains intact during light rain although the reflectivity is decreased from that before the rain. The method aims to provide a starting point for quantifying this effect without the need to manually process or annotate Doppler power spectrum images.

The method outlined here relies only on the co-polar Doppler velocity power spectrum, while the cross-polar Doppler velocity power spectrum and LDR are not used. Since insects can fall below the detectability threshold in the cross-polar velocity channel, vr_x and LDR are sometimes unavailable for non-precipitating clouds (as discussed in Williams et al., 2021). As such, if an LDR threshold is required to be met for classifying pixels as insects, this will necessarily result in removing some of the insect signal in the co-polar channel for range gates where Z_x is not reported.

Although the method is fairly crude, it shows promise and hopefully provides a useful first step towards improving our understanding of the impact of rain on insect migration. We tested more complex algorithms that include velocity texture parameters and LDR (following Williams et al., 2021). The goal of the Williams et al. (2021) algorithm is to classify each range gate as containing hydrometeors, insects or both; no attempt is made to separate overlapping insect and precipitation signals which is our goal here. When the data were also screened based on velocity texture parameter and LDR, the edges of regions of cloud and rainfall (in the spectral domain) were frequently misclassified as insects, as can also be seen in Fig. 8 of Williams et al. (2021). This is due to low precipitation fall speeds during drizzle or light rain, and this effect can be seen in Figure 7b,c when a higher v_t was used. In situations with light rain, the texture parameter algorithm of Williams et al. (2021) may provide a way forward.

A further issue is uncertainty related to attenuation of the radar beam during heavy rain. Millimetre-wavelength radars are designed for cloud rather than precipitation studies, and the beam can be strongly attenuated in rainfall (Lhermitte, 1990). Signal attenuation shows an almost linear relation to rainfall rate at Ka-band (Matrosov, 2005). Beam attenuation may limit the use of this method to examine insect flight during very heavy rain, but the impact of beam attenuation would depend on the rainfall rate and the height of the insect layer.

The main caveat to the method presented here is that the species of insect involved are unknown. Some inferences on taxa can be made based on the location, time of day and time of year. Citizen science or agricultural pest surveys can also be used to give information about the timing of large-scale movements. Due to the sampling strategy of the zenith-pointing cloud radar, further information on insect size or mass, horizontal flight speed or flight direction cannot be obtained without additional instrumentation. Research is ongoing to develop new processing tools to determine insect size and shape from WSR data (Melnikov et al., 2015), and

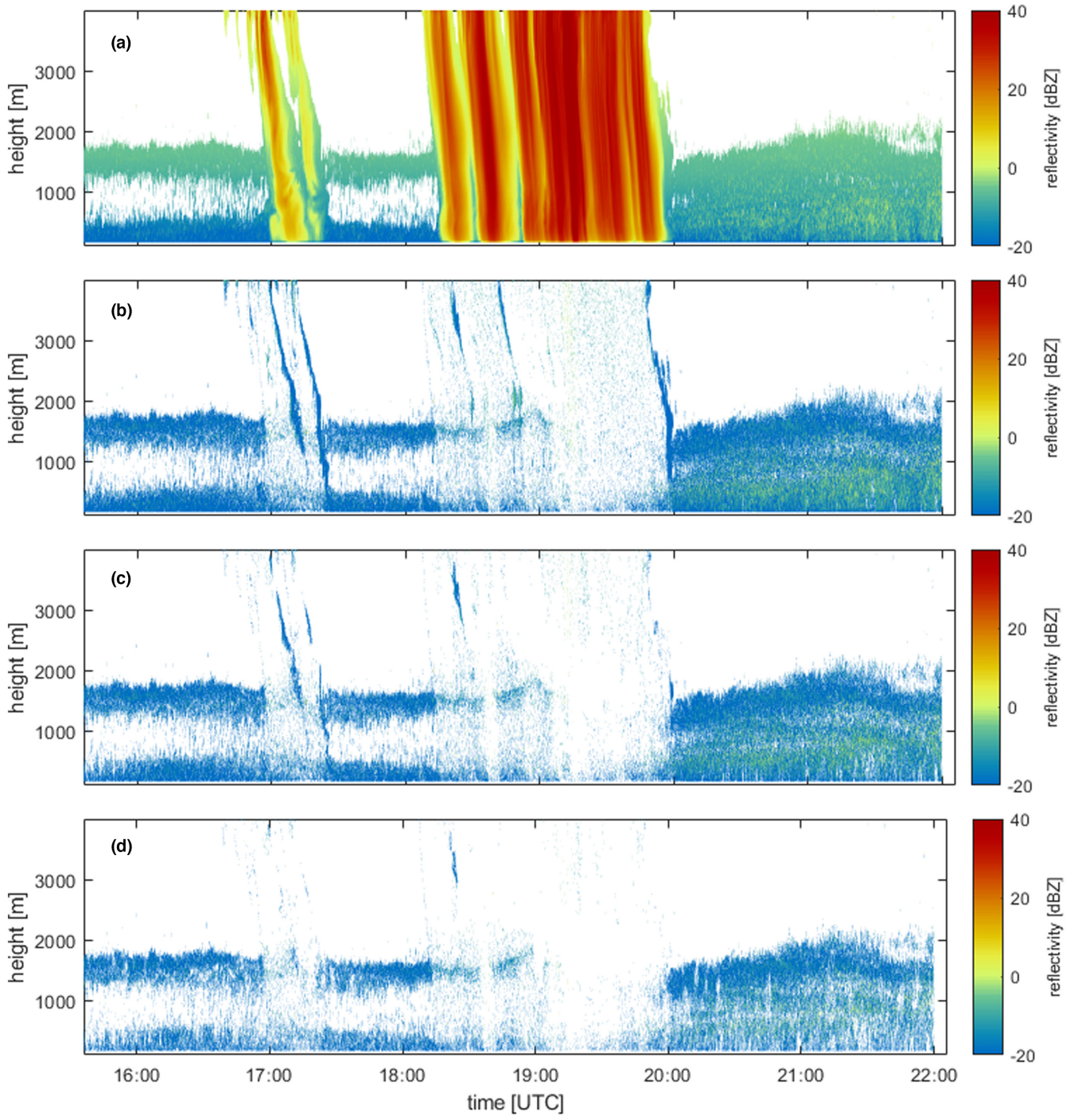

FIGURE 7 Time–height plots of reflectivity showing (a) total reflectivity; (b–d) show insect reflectivity when a threshold radial velocity values of ±2, ±1 and ±0.5 m/s, respectively.

so future studies may be able to combine WSR and cloud radar data to reveal more information on the insect taxa which migrate through rain. There is a clear need for further studies in which the insect species being impacted by raindrops is known, either in the laboratory (e.g. Dickerson et al., 2014) or by helikite or crewed aircraft studies (e.g. Dickison et al., 1983, 1986). In particular, future validation campaigns employing aerial insect sampling in rainy conditions may enable verification of radar-based techniques, providing metrics on algorithm performance such as probability of detection, false alarm rate and other measures of classification accuracy.

5 | CONCLUSIONS

Here we demonstrate a method that can be used to separate radar returns from insects and falling raindrops within a range gate in vertically pointing cloud radars. Although the method

presented is simple, the case study in Section 3 illustrates that it shows promise in distinguishing insects and falling rain. By applying the method to a case study with insects migrating at high altitude, we examined the ecologically significant issue of whether the insect continued flying during rain or if they were immediately 'washed out' or 'scrubbed' from the air by raindrops as suggested by Russell (1999). In the case in Section 3, the insect signal aloft clearly continues during rain although the reflectivity is diminished. As the rainfall rate increases around 19:15 (see Figure 7), the insect signal disappears; however, it is unclear whether this is due to insects falling out after impact with raindrops, choosing to descend or if the insect signal is still present but is masked by an increase in the noise floor.

There are several caveats to this method, which are described in detail in Section 4. It will not perform well during drizzle or very light rain when the mean vertical velocity of insects and raindrops overlaps, and without additional instrumentation or aerial sampling it is not possible to determine the species of insect flying. The insect species could be narrowed down by factoring in geographical and phenological factors, and citizen science data may also provide a useful metric for the timing of mass insect migration. Beam attenuation could limit the method performance during very heavy rain, and insects which are ascending or descending at rates beyond the threshold radial velocities (e.g. insects caught in strong updrafts/downdrafts) would be removed. Most of these issues arise from the automation procedure, particularly the selection of the threshold radial velocity. The insect signal is easily identified visually in Figure 6, so the data could be manually screened without the need to select a threshold velocity—although this would be time-consuming. As such, natural extensions to this method would be to employ automated spectral segmentation techniques such as those developed for mixed-phase cloud radar applications (e.g. Luke & Kollias, 2013; Radenz et al., 2019; Shupe et al., 2004). Despite these issues, it is clear from Figures 5–7 that insect migration at high altitude does not totally cease during rainfall, and that Doppler velocity spectra from millimetre-wavelength radars provide a unique way to examine insect flight through rainfall.

Future work should test the method presented here on a wider range of cases with varying rainfall rates. The theoretical analysis of Dickerson et al. (2014) demonstrated that the fate of insects struck by raindrops depends upon the relative mass and radius of the insect and the raindrop. Given a relationship between raindrop fall speed and diameter, if the vertical air motion is accounted for, then droplet size distribution can be inferred from the cloud radar data at each range gate. Droplet size distribution at ground level can also be assessed using a video disdrometer. For the case presented in Section 3, the maximum droplet diameter at ground level was approximately 2.5 mm (based on data from the collocated video disdrometer), while the insect size is unknown. Beyond these investigations on insect flight in the presence of rain, similar applications focusing on the flight of birds and bats in precipitating conditions may be constructed using this method as a foundation.

Despite decades of progress in entomology, relatively little is known about the typical migration height of many insect species, and how this varies spatially and under different meteorological conditions. Further advances in our understanding of insect migration will require combining data from WSR, which can show insect migration across scales of hundreds to thousands of kilometres (Stepanian et al., 2016) as well as revealing local aggregations (Stepanian et al., 2020; Tielens et al., 2021), with entomological radars that can provide information on insect size and shape (Chapman et al., 2003) or functional groups (Hao et al., 2020), and meteorological instrumentation that provides data on wind, temperature and rainfall. Here we have outlined a method for examining migratory insect flight during rain, adding to the growing body of literature utilizing cloud radar infrastructure to study insect behaviour. We hope that future efforts in this area will aid monitoring of long-range movements of insects, and serve to improve modelling efforts on aerial insect dispersal in realistic atmospheric conditions.

AUTHOR CONTRIBUTIONS

Conceptualization: Charlotte E. Wainwright; method development: Phillip M. Stepanian and Charlotte E. Wainwright; statistical analysis: Sabrina N. Volponi and Charlotte E. Wainwright; writing—first draft preparation: Charlotte E. Wainwright and Phillip M. Stepanian; writing—review and editing: Sabrina N. Volponi, Phillip M. Stepanian, Don R. Reynolds and David H. Richter.

ACKNOWLEDGEMENTS

Data were obtained from the Atmospheric Radiation Measurement (ARM) Climate Research Facility, a US. Department of Energy Office of Science user facility sponsored by the Office of Biological and Environmental Research. The colormap used throughout is based on Homeyer Rainbow (available in Py-ART) which was designed by Cameron Homeyer to be accessible to those with colour vision deficiency. Rothamsted Research receives grant-aided support from the UK Biotechnology and Biological Sciences Research Council. PMS is currently an MIT Lincoln Laboratory employee; no Laboratory funding or resources were used to produce the results/findings reported in this publication. The authors declare they have no conflicts of interest.

FUNDING INFORMATION

National Science Foundation Graduate Research Fellowship, grant number NSF DGE-1841556 (S.N.V); Richard and Peggy Notebaert Premier Fellowship (S.N.V); National Science Foundation Division of Emerging Frontiers, grant number 1840230 (P.M.S).

CONFLICT OF INTEREST

The authors declare they have no conflict of interest.

PEER REVIEW

The peer review history for this article is available at https://publons.com/publon/10.1111/2041-210X.14023.

DATA AVAILABILITY STATEMENT

The KAZR data used in this study are available at Atmospheric Radiation Measurement (ARM) user facility (2011), accessible via https://doi.org/10.5439/1025218. NEXRAD data are available at https://s3.amazonaws.com/noaa-nexrad-level2/index.html. An example MATLAB code demonstrating the method described in this manuscript to process cloud radar data to give total and insect reflectivity, as well as the cloud radar data for the case study shown in this manuscript, are available at DOI: https://doi.org/10.5281/zenodo.7110549 (Wainwright et al., 2022).

ORCID

Charlotte E. Wainwright https://orcid.org/0000-0002-9493-6285

REFERENCES

Atmospheric Radiation Measurement (ARM) User Facility. (2011). Ka ARM Zenith Radar (KAZRSPECCMASKGECOPOL). 2015-07-30 to 2015-07-30, Southern Great Plains (SGP) Central Facility, Lamont, OK (C1). Compiled by I. Lindenmaier, N. Bharadwaj, K. Johnson, D. Nelson, B. Isom, J. Hardin, A. Matthews, T. Wendler and V. Castro. ARM Data Center. Data set accessed 2021–10.

Banghoff, J. R., Sorber, J. D., Stensrud, D. J., Young, G. S., & Kumjian, M. R. (2020). A 10-year warm-season climatology of horizontal convective rolls and cellular convection in Central Oklahoma. *Monthly Weather Review*, *148*, 21–42.

Banghoff, J. R., Stensrud, D. J., & Kumjian, M. R. (2018). Convective boundary layer depth estimation from S-band dual-polarization radar. *Journal of Atmospheric and Oceanic Technology*, *35*, 1723–1733.

Boulanger, Y., Fabry, F., Kilambi, A., Pureswaran, D. S., Sturtevant, B. R., & Saint-Amant, R. (2017). The use of weather surveillance radar and high-resolution three dimensional weather data to monitor a spruce budworm mass exodus flight. *Agricultural and Forest Meteorology*, *234-235*, 127–135.

Browning, K. A., Nicol, J. C., Marsham, J. H., Rogberg, P., & Norton, E. G. (2011). Layers of insect echoes near a thunderstorm and implications for the interpretation of radar data in terms of airflow. *Quarterly Journal of the Royal Meteorological Society*, *137*, 723–735.

Burt, P. J., & Pedgley, D. E. (1997). Nocturnal insect migration: Effects of local winds. *Advances in Ecological Research*, *27*, 61–92.

Chandra, A. S., Kollias, P., Giangrande, S. E., & Klein, S. A. (2010). Long-term observations of the convective boundary layer using insect radar returns at the SGP ARM climate research facility. *Journal of Climate*, *23*, 5699–5714.

Chapman, J. W., Klaassen, R. H., Drake, V. A., Fossette, S., Hays, G. C., Metcalfe, J. D., Reynolds, A. M., Reynolds, D. R., & Alerstam, T. (2011). Animal orientation strategies for movement in flows. *Current Biology*, *21*, R861–R870.

Chapman, J. W., Reynolds, D. R., & Smith, A. D. (2003). Vertical-looking radar: A new tool for monitoring high-altitude insect migration. *Bioscience*, *53*, 503–511.

Delanoë, J., Protat, A., Vinson, J. P., Brett, W., Caudoux, C., Bertrand, F., Parent de Chatelet, J., Hallali, R., Barthes, L., Haeffelin, M., & Dupont, J. C. (2016). BASTA: A 95-GHz FMCW doppler radar for cloud and fog studies. *Journal of Atmospheric and Oceanic Technology*, *33*, 1023–1038.

Dickerson, A. K., Shankles, P. G., & Hu, D. L. (2014). Raindrops push and splash flying insects. *Physics of Fluids*, *26*, 027104.

Dickerson, A. K., Shankles, P. G., Madhavan, N. M., & Hu, D. L. (2012). Mosquitoes survive raindrop collisions by virtue of their low mass. *Proceedings of the National Academy of Sciences of the United States of America*, *109*, 9822–9827.

Dickison, R. B. B., Haggis, M. J., & Rainey, R. C. (1983). Spruce budworm moth flight and storms: Case study of a cold front system. *Journal of Climate and Applied Meteorology*, *22*, 278–286.

Dickison, R. B. B., Haggis, M. J., Rainey, R. C., & Burns, L. M. D. (1986). Spruce budworm moth flight and storms: Further studies using aircraft and radar. *Journal of Climate and Applied Meteorology*, *25*, 1600–1608.

Doviak, R. J., & Zrnić, D. S. (1993). *Doppler radar and weather observations* (2nd ed.). Academic Press.

Drake, V. A. (1982). Insects in the sea-breeze front at Canberra: A radar study. *Weather*, *37*, 134–143.

Drake, V. A. (1985). Radar observations of moths migrating in a nocturnal low-level jet. *Ecological Entomology*, *10*, 259–265.

Drake, V. A., & Farrow, R. A. (1985). A radar and aerial-trapping study of an early spring migration of moths (lepidoptera) in inland New South Wales. *Australian Journal of Ecology*, *10*, 223–235.

Drake, V. A., & Reynolds, D. R. (2012). *Radar entomology: Observing insect flight and migration*. CABI.

Franck, A., Moisseev, D., Vakkari, V., Leskinen, M., Lampilahti, J., Kerminen, V.-M., & O'Connor, E. (2021). Evaluation of convective boundary layer height estimates using radars operating at different frequency bands. *Atmospheric Measurement Techniques*, *14*, 7341–7353.

Geerts, B., & Miao, Q. (2005a). Airborne radar observations of the flight behavior of small insects in the atmospheric convective boundary layer. *Environmental Entomology*, *34*, 361–377.

Geerts, B., & Miao, Q. (2005b). The use of millimeter doppler radar echoes to estimate vertical air velocities in the fair-weather convective boundary layer. *Journal of Atmospheric and Oceanic Technology*, *22*, 225–246.

Greenbank, D. O., Schaefer, G. W., & Rainey, R. C. (1980). Spruce budworm (Lepidoptera: Tortricidae) moth flight and dispersal: New understanding from canopy observations, radar, and aircraft. *Memoirs of the Entomological Society of Canada*, *110*, 1–49.

Hao, Z., Drake, V. A., Taylor, J. R., & Warrant, E. (2020). Insect target classes discerned from entomological radar data. *Remote Sensing*, *12*, 673.

Helmus, J. J., & Collis, S. M. (2016). The python ARM radar toolkit (Py-ART), a library for working with weather radar data in the python programming language. *Journal of Open Research Software*, *4*, e25.

Hildebrand, P. H., & Sekhon, R. S. (1974). Objective determination of the noise level in Doppler spectra. *Journal of Applied Meteorology*, *13*, 808–811.

Hu, G., Lim, K. S., Horvitz, N., Clark, S. J., Reynolds, D. R., Sapir, N., & Chapman, J. W. (2016). Mass seasonal bioflows of high-flying insect migrants. *Science*, *354*, 1584–1586.

Hu, G., Lim, K. S., Reynolds, D. R., Reynolds, A. M., & Chapman, J. W. (2016). Wind-related orientation patterns in diurnal, crepuscular and nocturnal high-altitude insect migrants. *Frontiers in Behavioral Neuroscience*, *10*, 32.

Illingworth, A. J., Hogan, R. J., O'Connor, E. J., Bouniol, D., Brooks, M. E., Delanoë, J., Donovan, D. P., Eastment, J. D., Gaussiat, N., Goddard, J. W. F., Haeffelin, M., Klein Baltnik, H., Krasnov, O. A., Pelon, J., Piriou, J.-M., Protat, A., Russchenberg, H. W. J., Seifert, A., Tompkins, A. M., … Wrench, C. L. (2007). CLOUDNET: Continuous evaluation of cloud profiles in seven operational models using ground-based observations. *Bulletin of the American Meteorological Society*, *88*, 883–898.

Jatau, P., Melnikov, V., & Yu, T. Y. (2021). A machine learning approach for classifying bird and insect radar echoes with S-band polarimetric weather radar. *Journal of Atmospheric and Oceanic Technology*, *38*, 1797–1812.

Kalapureddy, M. C. R., Sukanya, P., Das, S. K., Deshpande, S. M., Pandithurai, G., Pazamany, A. L., Jha Ambuj, K., Chakravarty, K., Kalekar, P., Krishna Devisetty, H., & Annam, S. (2018). A simple biota removal algorithm for 35GHz cloud radar measurements. *Atmospheric Measurement Techniques*, *11*, 1417–1436.

Kollias, P., Clothiaux, E. E., Ackerman, T. P., Albrecht, B. A., Widener, K. B., Moran, K. P., Luke, E. P., Johnson, K. L., Bharadwaj, N., Mead, J. B., Miller, M. A., Verlinde, J., Marchand, R. T., & Mace, G. G. (2016). Development and applications of ARM millimeter-wavelength cloud radars. *Meteorological Monographs*, *57*, 1–17.

Lamer, K., & Kollias, P. (2015). Observations of fair-weather cumuli over land: Dynamical factors controlling cloud size and cover. *Geophysical Research Letters*, *42*, 8693–8701.

Leibold, M. A., Holyoak, M., Mouquet, N., Amarasekare, P., Chase, J. M., Hoopes, M. F., Holt, R. D., Shurin, J. B., Law, R., Tilman, D., Loreau, M., & Gonzalez, A. (2004). The metacommunity concept: A framework for multi-scale community ecology. *Ecology Letters*, *7*, 601–613.

Leskinen, M., Markkula, I., Koistinen, J., Pylkkö, P., Ooperi, S., Siljamo, P., Ojanen, H., Raiskio, S., & Tiilikkala, K. (2011). Pest insect immigration warning by an atmospheric dispersion model, weather radars and traps. *Journal of Applied Entomology*, *135*, 55–67.

Lhermitte, R. (1990). Attenutation and scattering of millimeter wavelength radiation by clouds and precipitation. *Journal of Atmospheric & Oceanic Technology*, *7*, 464–479.

Luke, E. P., & Kollias, P. (2013). Separating cloud and drizzle radar moments during precipitation onset using Doppler spectra. *Journal of Atmospheric and Oceanic Technology*, *30*, 1656–1671.

Luke, E. P., Kollias, P., Johnson, K. L., & Clothiaux, E. E. (2008). A technique for the automatic detection of insect clutter in cloud radar returns. *Journal of Atmospheric and Oceanic Technology*, *25*, 1498–1513.

Markkula, I., Ojanen, H., Tiilikkala, K., Raiskio, S., Pylkkö, P., & Koistinen, J. (2008). Insect migration case study by polarimetric radar. In *Proceedings of the fifth European conference on radar in meteorology and hydrology (ERAD 2008) Helsinki, Finland, 30 June–4 July 2008* (p. 5). Finnish Meteorological Institute.

Martner, B. E., & Moran, K. P. (2001). Using cloud radar polarization measurements to evaluate stratus cloud and insect echoes. *Journal of Geophysical Research*, *106*, 4891–4897.

Matrosov, S. Y. (2005). Attenuation-based estimates of rainfall rates aloft with vertically pointing ka-band radars. *Journal of Atmospheric and Oceanic Technology*, *22*, 43–54.

Melnikov, V. M., Istok, M. J., & Westbrook, J. K. (2015). Asymmetric radar echo patterns from insects. *Journal of Atmospheric and Oceanic Technology*, *32*, 659–674.

Radenz, M., Bühl, J., Seifert, P., Griesche, H., & Engelmann, R. (2019). PeakTree: A framework for structure-preserving radar Doppler spectra analysis. *Atmospheric Measurement Techniques*, *12*, 4813–4828.

Rennie, S. J. (2014). Common orientation and layering of migrating insects in southeastern Australia observed with a Doppler weather radar. *Meteorological Applications*, *21*, 218–229.

Reynolds, D. R., Chapman, J. W., & Drake, V. A. (2018). Riders on the wind: The aeroecology of insect migrants. In P. B. Chilson, W. F. Frick, J. F. Kelly, & F. Liechti (Eds.), *Aeroecology* (pp. 145–178). Springer International Publishing.

Russell, R. W. (1999). Precipitation scrubbing of aerial plankton: Inferences from bird behavior. *Oecologia*, *118*, 381–387.

Russell, R. W., & Wilson, J. W. (1997). Radar-observed "fine lines" in the optically clear boundary layer: Reflectivity contributions from aerial plankton and its predators. *Boundary-Layer Meteorology*, *82*, 235–262.

Satterfield, D. A., Sillett, T. S., Chapman, J. W., Altizer, S., & Marra, P. P. (2020). Seasonal insect migrations: Massive, influential, and overlooked. *Frontiers in Ecology and the Environment*, *18*, 335–344.

Shupe, M. D., Kollias, P., Matrosov, S. Y., & Schneider, T. L. (2004). Deriving mixed-phase cloud properties from Doppler radar spectra. *Journal of Atmospheric and Oceanic Technology*, *21*, 660–670.

Sisterton, D. L., Peppler, R. A., Cress, T. S., Lamb, P. J., & Turner, D. D. (2016). The ARM southern Great Plains (SGP) site. *Meteorological Monographs*, *57*, 6.1–6.14.

Stepanian, P. M., Chilson, P. B., & Kelly, J. F. (2014). An introduction to radar image processing in ecology. *Methods in Ecology and Evolution*, *5*, 730–738.

Stepanian, P. M., Entrekin, S. A., Wainwright, C. E., Mirkovic, D., Tank, J. L., & Kelly, J. F. (2020). Declines in an abundant aquatic insect, the burrowing mayfly, across major north American waterways. *Proceedings of the National Academy of Sciences of the United States of America*, *117*, 2987–2992.

Stepanian, P. M., Horton, K. G., Melnikov, V. M., Zrnić, D. S., & Gauthreaux, S. A. (2016). Dual-polarization radar products for biological applications. *Ecosphere*, *7*, e01539.

Sturtevant, B. R., Achtemeier, G. L., Charney, J. J., Anderson, D. P., Cooke, B. J., & Townsend, P. A. (2013). Long-distance dispersal of spruce budworm (Choristoneura fumiferana Clemens) in Minnesota (USA) and Ontario (Canada) via the atmospheric pathway. *Agricultural and Forest Meteorology*, *168*, 186–200.

Tielens, E. K., Cimprich, P. M., Clark, B. A., DiPilla, A. M., Kelly, J. F., Mirkovic, D., Strand, A. I., Zhai, M., & Stepanian, P. M. (2021). Nocturnal city lighting elicits a macroscale response from an insect outbreak population. *Biology Letters*, *17*, 20200808.

Wainwright, C. E., Reynolds, D. R., & Reynolds, A. M. (2020). Linking small-scale flight manoeuvers and density profiles to the vertical movement of insects in the nocturnal stable boundary layer. *Scientific Reports*, *10*, 1019.

Wainwright, C. E., Stepanian, P. M., Reynolds, D. R., & Reynolds, A. M. (2017). The movement of small insects in the convective boundary layer: Linking patterns to processes. *Scientific Reports*, *7*, 5438.

Wainwright, C. E., Volponi, S. N., Stepanian, P. M., Reynolds, D. R., & Richter, D. H. (2022). Code/data to accompany publication "using cloud radar to investigate the effect of rainfall on migratory insect flight" [data set]. Methods in Ecology and Evolution (version 1). *Zenodo*. https://doi.org/10.5281/zenodo.7110549

Williams, C., Johnson, K., Giangrande, S., Hardin, J., Öktem, R., & Romps, D. (2021). Identifying insects, clouds, and precipitation using vertically pointing polarimetric radar Doppler velocity spectra. *Atmospheric Measurement Techniques*, *14*, 4425–4444.

Williams, C. R., Maahn, M., Hardin, J. C., & De Boer, G. (2018). Clutter mitigation, multiple peaks, and high-order spectral moments in 35 GHz vertically pointing radar velocity spectra. *Atmospheric Measurement Techniques*, *11*, 4963–4980.

Wood, C. R., O'Connor, E. J., Hurley, R. A., Reynolds, D. R., & Illingworth, A. J. (2009). Cloud-radar observations of insects in the UK convective boundary layer. *Meteorological Applications*, *116*, 491–500.

Wotton, K. R., Gao, B., Menz, M. H., Morris, R. K., Ball, S. G., Lim, K. S., Reynolds, D. R., Hu, G., & Chapman, J. W. (2019). Mass seasonal migrations of hoverflies provide extensive pollinsation and crop protection services. *Current Biology*, *29*, 2167–2173.

How to cite this article: Wainwright, C. E., Volponi, S. N., Stepanian, P. M., Reynolds, D. R., & Richter, D. H. (2023). Using cloud radar to investigate the effect of rainfall on migratory insect flight. *Methods in Ecology and Evolution*, *14*, 655–668. https://doi.org/10.1111/2041-210X.14023